

The Probability Distribution of the Thorpe Displacement within OvertURNS in Juan de Fuca Strait

KATE STANSFIELD,* CHRIS GARRETT, AND RICHARD DEWEY

School of Earth and Ocean Sciences, University of Victoria, Victoria, British Columbia, Canada

(Manuscript received 9 November 2000, in final form 19 April 2001)

ABSTRACT

Vertical mixing in the ocean can sometimes be quantified by measurements of the Thorpe overturning scale, L_T . In regions of weak mixing and weak density gradients such measurements may be limited by slow sensor response times (or sampling rates) and/or by lack of resolution and noise in the density measurements. On the other hand, the Thorpe scale can be written as $L_T = (\int_0^\infty L^2 P_1(L) dL)^{1/2}$, where $P_1(L)$ is the probability of the Thorpe displacement, L . Data from Juan de Fuca Strait, British Columbia, show that, even though the probability of a small Thorpe displacement is much greater than that of a large Thorpe displacement, it is the large and more easily resolved values of L that dominate the Thorpe scale. It is found to be possible to determine L_T down to a scale of 0.4 m with a conventional conductivity–temperature–depth instrument. This corresponds to values of $K_v \approx 10^{-4} \text{ m}^2 \text{ s}^{-1}$ in summertime if $L_T \approx (\epsilon/N^3)^{1/2}$, as is confirmed using velocity and temperature microstructure data. Here $P_1(L)$ is a convolution of the probability distribution of overturn height, $P_2(H)$, with the probability distribution of the fractional displacement within each overturn, $P_3(L/H)$. Data show that $P_2(H)$ is dominated by small overturns, consistent with previous work on the thickness of turbulence patches. Finally, the distribution of $P_3(L/H)$ is examined and compared with the prediction of a very simple kinematic model. The data show a pattern similar to that predicted by the model, though with more small L/H and fewer medium to large L/H than in the model.

1. Introduction

Small-scale mixing is crucial in many important issues from global climate to marine productivity. The processes responsible for the mixing cannot generally be resolved in numerical models so their effects are usually parameterized, often with no spatial or temporal dependence. Measuring the vertical mixing rate K_v is essential for checking proposed parameterizations and for direct application.

A technique proposed by Thorpe (1977) involves the observation of density overturns. The Thorpe scale, or vertical overturning scale L_T , is defined as the root mean square (rms) of the vertical displacements, or Thorpe displacements L , required to reorder a measured profile of potential density so that it is gravitationally stable. If the Ozmidov scale (Ozmidov 1965) $L_O = 0.8L_T$ as found by Dillon (1982) and the mixing efficiency $\Gamma = 0.2$ (e.g., Oakey 1982), then the vertical diffusivity

$K_v \approx 0.1NL_T^2$, where N is the buoyancy frequency of the reordered density profile.

Unfortunately, use of this technique usually requires either a large vertical density gradient and stronger mixing than is typically found in the open ocean, or more sensitive instruments than a conventional conductivity–temperature–depth (CTD) instrument (e.g., Mudge and Lueck 1994). The vertical mixing rate is therefore more often determined by velocity or temperature microstructure measurements. Here we revisit the possibility of determining Thorpe scales from potential density data derived from measurements taken using a CTD in an estuarine environment where the density gradients are large and where mixing rates are typically larger than in the open ocean.

The probability distribution of L in some simple, idealized overturns is examined in the next section, and the ability of three different CTD instruments to measure L is discussed in section 3. In section 4 we describe the collection and processing of CTD data in Juan de Fuca Strait and present the resulting probability distributions of L . Section 5 combines our results from the CTD data with some complementary microstructure velocity shear and temperature data to confirm a previously determined relationship (e.g., Dillon 1982; Crawford 1986) between L_T and the Ozmidov scale. Finally, in section 6, we explore the probability distribution of L/H within over-

* Current affiliation: James Rennell Division, Southampton Oceanography Centre, University of Southampton, Southampton, United Kingdom.

Corresponding author address: Kate Stansfield, James Rennell Division, Southampton Oceanography Centre, University of Southampton, European Way, Southampton, SO14 3ZH, United Kingdom.
E-mail: Kate.L.Stansfield@soc.soton.ac.uk

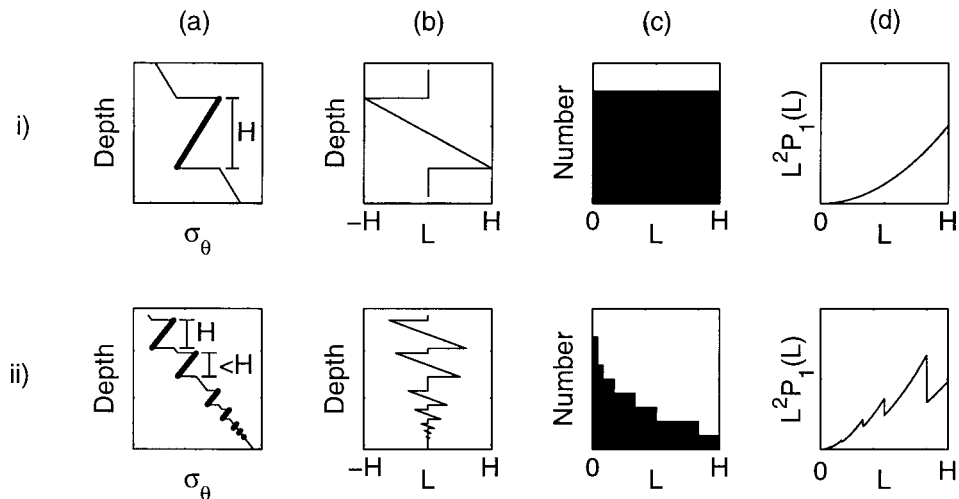


FIG. 1. (a) Hypothetical potential density profiles, σ_θ , including idealized, arbitrary, overturns. The thick line shows the overturning regions, where $L \neq 0$. (b) Profiles of the corresponding L , (c) histogram of L (the occurrence of $L = 0$ has not been plotted), and (d) $L^2 P_1(L)$.

turns of height H and compare the measured distribution with that for a simple kinematic model.

2. The probability distribution of the Thorpe displacement

The vertical overturning scale may be written as

$$L_T = \left(\int_0^\infty L^2 P_1(L) dL \right)^{1/2}, \quad (1)$$

where $P_1(L)$ is the probability distribution of L over a profile. As L is squared in (1), large displacements are more important than small displacements for determining L_T provided that the distribution of $P_1(L)$ falls off less steeply than $1/L^3$.

To illustrate the application of (1), we consider the distribution of L arising from some simple overturns superimposed on a linear potential density profile (see Fig. 1). The two cases examined are (i) a single, large overturn and (ii) multiple overturns of arbitrary, and varying, vertical extent. Note that the occurrence of L equal to zero has not been plotted in the histograms; zero L is most probable as it represents the parts of the water column that are not overturning (stably stratified).

In case (i), that of the single, large, simple overturn, the distribution of L is flat and $L^2 P_1(L)$ increases with increasing L . In case (ii), the distribution of L is simply a sum of overturns, and so is critically dependent on the number, and vertical extent, of the overturns chosen.

Since L_T can be computed as the square root of the integral of $L^2 P_1(L)$, these examples suggest that, even in a profile containing multiple small overturns, small values of L may contribute little to the magnitude of L_T . Two other relevant quantities are defined here: (i) the probability distribution $P_2(H)$ of the overturn height

H and (ii) the probability distribution $P_3(L/H)$ of L within an overturn. These quantities are related to $P_1(L)$ by

$$P_1(L) = \int_0^\infty H P_3(L/H) P_2(H) dH \bigg/ \int_0^\infty H^2 P_2(H) dH, \quad (2)$$

where the denominator is determined from the requirement that $\int_0^\infty P_1(L) dL = 1$ and we have assumed that $P_3(L/H)$ is independent of H . We will later consider $P_3(L/H)$ using a simple model and for a real dataset, but first we consider the limitations of determining L with some conventional CTD instruments.

3. CTD instrument resolution of Thorpe displacements

The accuracy with which each L can be measured using a CTD profiler depends on the noise level of the measured potential density profile compared with the background, or mean, vertical potential density gradient. The relative importance of depth and density resolution for a particular CTD can be estimated from

$$R = \frac{d\rho/dz \Delta z_{\text{inst}}}{dz \Delta \rho_{\text{inst}}}, \quad (3)$$

where $d\rho/dz$ is the background density gradient and Δz_{inst} and $\Delta \rho_{\text{inst}}$ are the instrument depth (pressure) and density resolution, respectively. The value of R for a particular instrument determines which measurement, pressure or density, limits the resolvable density structure. If $R > 1$, resolution of the pressure is the limiting factor, whereas if $R < 1$ it is the density measurement that restricts the resolution of the density profile.

Table 1 gives the value of R for three different CTD instruments based on the manufacturer's specifications

TABLE 1. Value of the parameter R for three different CTD instruments under two different stratification regimes in Juan de Fuca Strait. If $R > 1$, resolution of the pressure is the limiting factor, whereas if $R < 1$ it is the density measurement that restricts the resolution of the density profile.

Instrument and manufacturers' specifications ^(a)	R value	
	(winter) $\frac{1}{\rho} \frac{dp}{dz} \approx 1.0 \times 10^{-5} \text{ m}^{-1}$	(summer) $\frac{1}{\rho} \frac{dp}{dz} \approx 3.0 \times 10^{-5} \text{ m}^{-1}$
Applied Microsystems, Ltd. STD 12 plus		
Sampling rate = 15 s^{-1}	0.32	0.95
$\Delta z = 0.07 \text{ m}^{(b)} + 0.05 \text{ m}^{(c)} = 0.12 \text{ m}$		
$\Delta T = 0.001^\circ\text{C}$		
$\Delta C = 0.0003 \text{ S m}^{-1}$		
$\Delta \rho = 0.0038 \text{ kg m}^{-3}$		
Sea-Bird Electronics, Inc. 911plus		
Sampling rate = 24 s^{-1}	1.83	5.50
$\Delta z = 0.04 \text{ m}^{(b)} + 0.07 \text{ m}^{(c)} = 0.11 \text{ m}$		
$\Delta T = 0.0002^\circ\text{C}$		
$\Delta C = 0.00004 \text{ S m}^{-1}$		
$\Delta \rho = 0.0006 \text{ kg m}^{-3(d)}$		
Sea-Bird Electronics, Inc. Seacat 19		
Sampling rate = 2 s^{-1}	2.41	7.23
$\Delta z = 0.50 \text{ m}^{(b)} + 0.03 \text{ m}^{(c)} = 0.53 \text{ m}$		
$\Delta T = 0.001^\circ\text{C}$		
$\Delta C = 0.0001 \text{ S m}^{-1}$		
$\Delta \rho = 0.0022 \text{ kg m}^{-3(d)}$		

^(a) Sensor resolutions are based on the manufacturer's specifications.

^(b) Vertical resolutions are additionally based on the assumption of a 1 m s^{-1} descent rate. In the case of the SBE with pumped temperature–conductivity ducts, the resulting vertical resolution is that specified by the manufacturer for a 1 m s^{-1} descent rate (Sea-Bird Electronics, Inc., Application Note No. 38, 1992).

^(c) Based on the manufacturer's specification and the full scale depth range of the pressure sensor used. The SBE 911plus CTD had a full scale pressure range of 10 000 psi absolute $\approx 6730 \text{ m}$. The AML STD 12 plus had a full scale pressure range of 1000 dbar $\approx 990 \text{ m}$. The SBE Seacat 19 had a full-scale pressure range of 300 psi absolute $\approx 205 \text{ m}$.

^(d) The resulting density resolution of each instrument is calculated assuming a temperature–conductivity–pressure space based on the extreme values measured in Juan de Fuca Strait in Feb and Aug 1998 and using the nonlinear equations of state (Fofonoff and Millard 1983). The ranges used were $6.7\text{--}12.7^\circ\text{C}$, $3.2\text{--}3.8 \text{ S m}^{-1}$, and $0\text{--}170 \text{ dbar}$, respectively.

and on the mean potential density gradients observed in Juan de Fuca Strait in February and August 1998. The Sea-Bird Electronics, Inc. (SBE) 911plus CTD, Seacat 19 CTD, and Applied Microsystems Ltd. (AML) STD 12 plus CTD were chosen because they are representative of equipment readily available to us.

In choosing the depth resolution (Δz for Table 1) we have taken one contribution to be the sampling interval times a typical descent rate of 1 m s^{-1} . We have then added a second contribution corresponding to the resolution of the pressure sensor. We realize that by assuming a slowly varying descent the limitation by the pressure sensor resolution could be removed. Doing this would reduce the value of R in Table 1, particularly for the SBE 911plus.

The ratio R is also reduced below the value shown in Table 1 if one assumes that the appropriate value of $\Delta \rho$ is the instrument noise. Instrument noise may be several times the resolution but its effect could be reduced by vertical averaging, albeit at the expense of vertical resolution.

Examining the values of R in Table 1 and taking the above considerations into account, our conclusion is that

detection of overturns using the AML STD 12 plus is limited by the sampling rate (and hence, presumably, the sensor time constants). For the Sea-Bird instruments, the limitation comes from both the time constants and the density resolution, though in summer the time constant is a more serious constraint than the density resolution and noise. While one may sometimes have the ability to increase the depth resolution, without loss of data quality, by varying the profiling rate, one cannot usually alter the density resolution of a particular CTD. A modest limitation by the depth resolution is thus preferable to a limitation by the density resolution.

4. Distributions of Thorpe displacements in overturns from CTD data collected in Juan de Fuca Strait

a. Juan de Fuca Strait

Juan de Fuca Strait separates southern Vancouver Island from the northern coast of Washington State (see Fig. 2). It is a fairly straight-sided channel, about 100 km long and 20 km wide, with water depths of less than

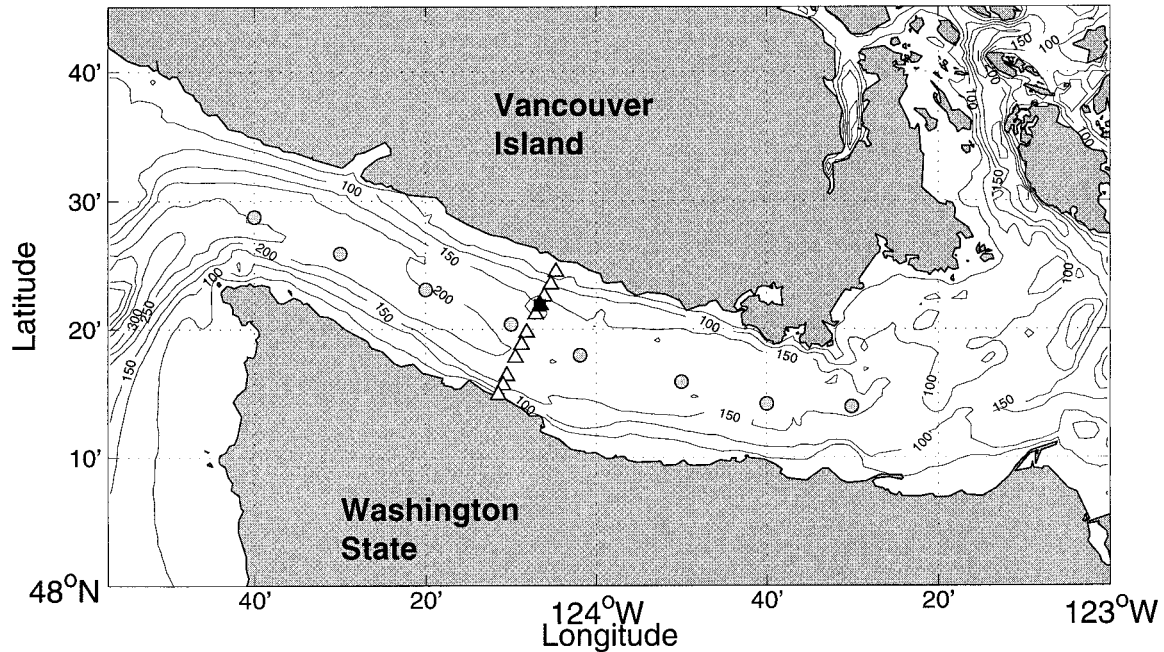


FIG. 2. Map showing Juan de Fuca Strait, bathymetric contours, and CTD station positions; C-line stations are shown as triangles, A-line stations are shown as shaded circles, and the time series station is shown as a filled square.

200 m except at the western mouth where depths reach 250 m. The strait receives much of the freshwater runoff from southern British Columbia and northern Washington State, via Georgia Strait and Puget Sound. In particular, it is the main conduit of the Fraser River discharge to the Pacific Ocean.

The strait is stratified with the largest stratification (and vertical salinity variation) occurring in summer, coincident with the peak of the Fraser River discharge and the period of southeastward coastal winds (upwelling favorable). Tides within the strait are mixed, mainly semidiurnal with tidal currents of about 1 m s^{-1} . The strait is affected by rotation and has a strong (estuarine) shear flow with a mean flow Richardson number of about 5 in August, depending on the magnitude of the seasonal mean shear flow.

b. Instruments and data collection

The winter CTD data used in this paper were collected on 22 and 23 February 1998 using a SBE 911plus CTD aboard the Research Vessel *Thomas G. Thompson*, cruise designation Tn075. Casts were made at 10 stations on a transect across Juan de Fuca Strait (C line) (see Fig. 2).

Summer data were collected on 31 July and 1 and 2 August using a SBE 911plus CTD aboard the Canadian Coast Guard Vessel *Vector*, cruise designation 9834. Casts were made at 57 stations, including two repetitions of an across-strait transect (C line), one along-strait transect (A line), and a 24-h, hourly, time series at $124^{\circ}07'W$, $48^{\circ}22'N$ (see Fig. 2).

Both SBE 911plus CTD instruments had a sampling rate of 24 s^{-1} and had dual temperature and conductivity sensor packages. In February the CTD was lowered at a rate of 0.5 m s^{-1} and in August the rate was 0.75 m s^{-1} . In both February and August flow through the conductivity cells was pumped. This maintains a steady flow rate of $30 \text{ cm}^3 \text{ s}^{-1}$ through the cell and leads to an effective delay of 0.073 s in the response of the conductivity cell relative to the temperature sensor. This is corrected in real time by the SBE 11plus deck unit.

c. Data processing

The data were corrected for the short-term mismatch of the sensor responses (Lueck and Picklo 1990; Morison et al., 1994) in order to minimize sharp spikes in salinity and density. Corrections were also made for the long-term thermal lag of the conductivity cell (Lueck and Picklo 1990; Morison et al. 1994).

The effect of ship and vertical CTD package motion was removed from each cast by only keeping data for the first occurrence of a pressure greater than all pressures previously encountered. This ensured that the records contained no depth reversals (although the weather was calm for all casts and depth reversals were infrequent). Any spikes remaining in the conductivity and temperature data were removed by calculating the 25-point running mean and using this to replace values that were further away than three times the standard deviation defined over the same 25 points. Spikes were infrequent in our datasets. The despiked temperature and conductivity signals were then used to construct poten-

tial density profiles for the midwater region, avoiding the surface and bottom mixed layers. An upper depth limit of 20 m was used, as this was the maximum depth of the surface mixed layer. The depth of the bottom mixed layer was determined separately for each profile. By calculating the values of L_T based on the potential density profile, instead of the temperature profile, we eliminate the problem of spurious temperature overturns caused by salinity-compensated intrusions.

The method of Galbraith and Kelley (1996, hereafter GK) was then applied to the data to identify overturning regions and the Thorpe scale was calculated. There are other techniques for determining Thorpe scales from CTD data (e.g., Ferron et al. 1998; Alford and Pinkel 2000) but the method of GK appears particularly robust. Galbraith and Kelley essentially apply two tests to unstable regions in any potential density profile to try and distinguish false density inversions caused by noisy CTD data from real overturning regions. First, they establish a “run-length” criterion whereby the probability density function of the length of adjacent positive or negative values (runs) in the profile of the Thorpe fluctuation, $\rho' = \rho(z) - \hat{\rho}(z)$, is compared with the probability density function of random noise (i.e., an independent repeated Bernoulli trial). Overturning regions with “run-lengths” less than a noise threshold value are rejected. Second, they test the T - S relationship of the overturning region and reject regions where the T - S relationship is not “tight.” This is done as follows: within each reordering region they perform a linear least squares fit for each of temperature and salinity to the observed potential density. They then calculate the root-mean-square value of the difference between the observed potential density and the straight line fits for temperature and salinity. These quantities are then non-dimensionalized by the rms value of the Thorpe fluctuation density within the same reordering region. Overturns where the maximum of this ratio (for either temperature or salinity) exceeds 0.5 are rejected. Such overturns are judged by GK to be reordering regions that have insufficiently tight T - S relationships to be regarded as signatures of overturning motions. The reader is referred to GK for further details of the method.

Values of L_T were calculated from the profiles of L using only those overturning regions positively identified by the GK method. Thorpe scales were calculated for the entire midwater region ($L_{T_{wc}}$) for each profile, as well as for individual overturns ($L_{T_{ovt}}$), where an overturn is defined as a gravitationally unstable region of the profile over which the values of L sum to zero.

The ability of the method of GK to reject spurious overturning regions was tested by applying the method to some of our observed potential density profiles that had (i) been reordered so as to be gravitationally stable and (ii) had profiles of random noise, with a normal distribution and a standard deviation of 0.002 kg m^{-3} , added to them. The GK method detected no overturning regions that passed both tests. It thus seems likely that

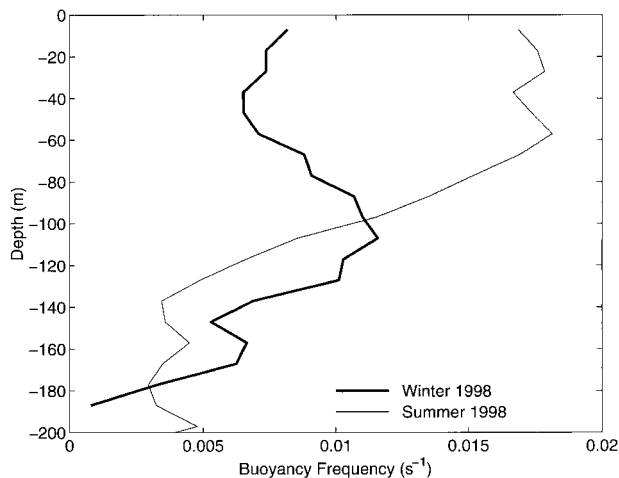


FIG. 3. Profiles of mean buoyancy frequency, N (s^{-1}).

the GK method does not accept false overturns. It is possible that the method rejects some true overturns, but these are likely to be small ones that do not contribute greatly to L_T . We will later compare the values of L_T obtained with and without application of the GK method.

d. Results

Figure 3 shows the mean profile of buoyancy frequency, N (s^{-1}), for February and August calculated at 10-m depth intervals from sorted temperature, salinity, and pressure profiles. The mean-flow Richardson number was estimated to be 5.8 in August. This was calculated using the maximum shear (between 30 and 90 m) of the along-channel component of the time-averaged mean flow and the mean value of N over the same depth interval. The mean flow profile was derived from a 28-day record (3–31 July) of velocities measured by a bottom mounted acoustic Doppler current profiler (ADCP) using 4-m bins and the mean value of N was determined from the August CTD profiles using 10-m bins. Unfortunately we have no velocity data for February.

Examples of typical cleaned potential density profiles, the corresponding L profiles, and the same L profiles after applying the method of GK are shown in Fig. 4, one set of profiles each for the winter and summer datasets.

For the February dataset the method of GK found 36 overturns and gave an rms $L_{T_{wc}}$ of 0.77 m for the primary sensor pair (CT1). The data from the secondary sensor pair (CT2) contained the same number of overturns but gave an rms $L_{T_{wc}}$ of 0.81 m. The reader is reminded that $L_{T_{wc}}$ includes the parts of the water column where $L = 0$, between overturning regions. Values of $L_{T_{ovt}}$ ranged from 0.1 to 4.5 m for CT1 and from 0.12 to 4.6 m for CT2. Without applying the method of GK, the rms $L_{T_{wc}}$ was 1.09 m for CT1 and 1.02 m for CT2.

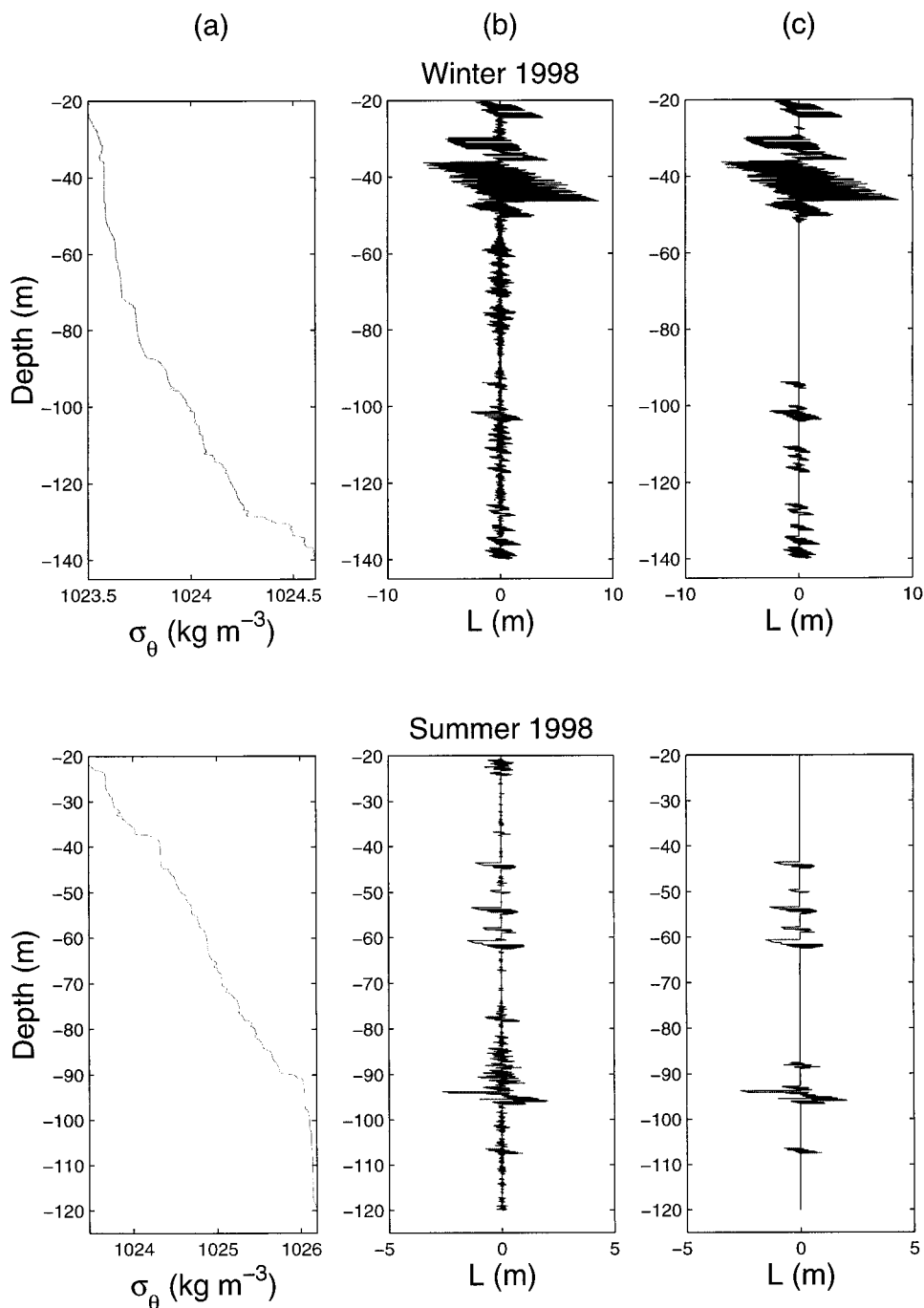


FIG. 4. (a) Cleaned potential density profile, (b) profile of L , and (c) profile of L after processing the data using the method of Galbraith and Kelley (1996). The three upper panels show an example from the winter dataset; the three lower panels show an example of the summer data. Not all the overturning regions in the density profiles show up clearly due to the large density range and the resolution of the figure.

For the summer data, the method detected 345 overturns in the data from CT1, with an rms $L_{T_{wc}}$ of 0.45 m, and 329 overturns from the CT2 data with an rms $L_{T_{wc}}$ of 0.46 m. Values of $L_{T_{ovt}}$ ranged from 0.03 m to 5.1 m for CT1 and from 0.14 to 5.1 m for CT2. Without

the restrictions of GK the rms $L_{T_{wc}}$ was 0.52 m for CT1 and 0.55 m for CT2.

The vertical distribution of $L_{T_{ovt}}$ for both datasets using CT1 is shown in Fig. 5. Here $L_{T_{ovt}}$ is plotted as a constant over the vertical extent of each overturn. In

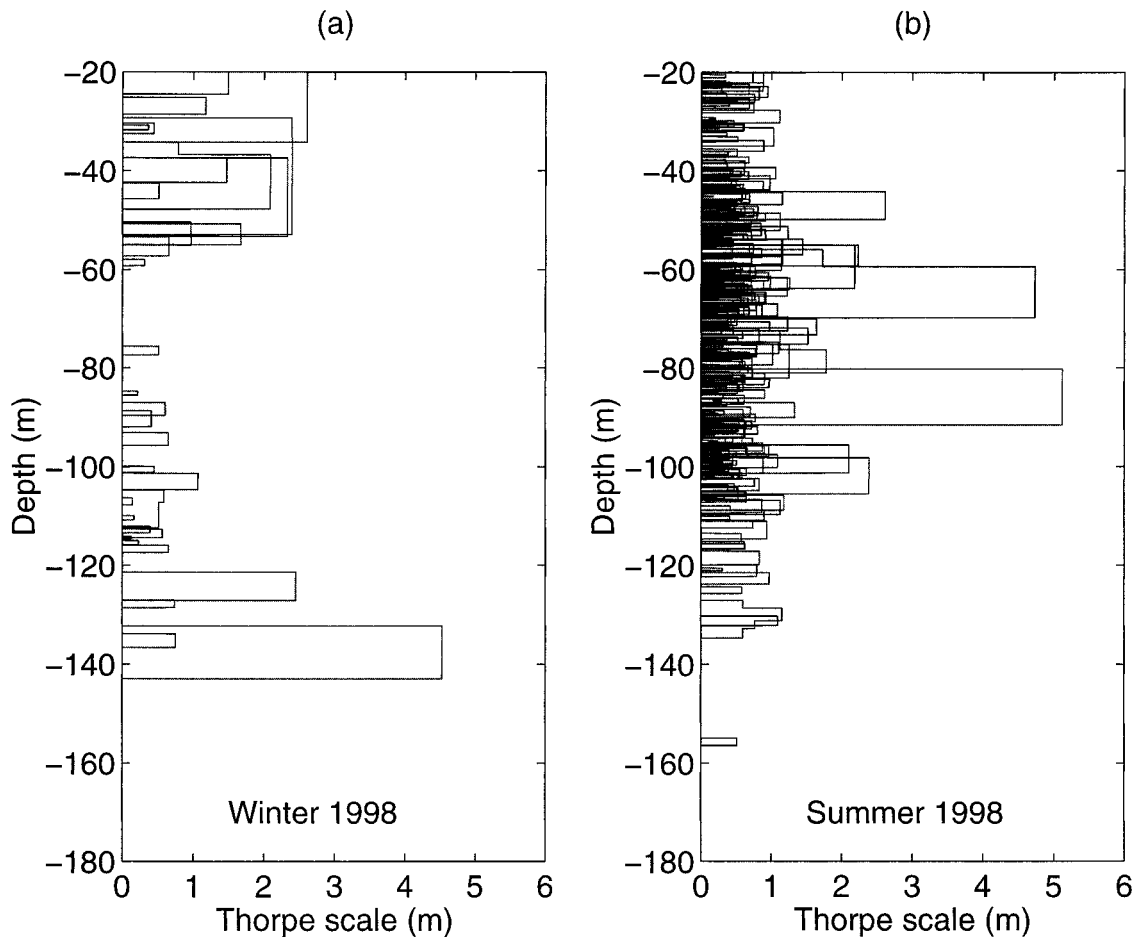


FIG. 5. Depth distribution of L_{Tovt} for (a) winter overturns from 10 casts and (b) summer overturns from 57 casts. The depth of each horizontal bar indicates the vertical extent of the overturn; the magnitude of L_{Tovt} is indicated by the length of each bar.

February, large overturns occurred between 20 and 60 m and between 120 and 140 m, while in August there were large overturns in the middle of the water column. This may be due to a stronger mean shear in summer as a consequence of the peak in the discharge of the Fraser River. The small to medium overturns were fairly evenly distributed.

Figures 6a and 6b show the probability distributions $P_1(L)$ of L and $L^2 P_1(L)$ for the winter and summer datasets. Note that the distribution of $L^2 P_1(L)$ increases with increasing L , as in Fig. 1d, row ii.

On the suggestion of a referee, we have also checked whether L is lognormally distributed, as might be expected if, as proposed for the turbulent dissipation rate, L arises from a multiplicative series of independent events (e.g., Frisch 1995). The distribution of $\log_{10}(L)$ shown in Fig. 6c spans 2.6 decades in winter and 3.3 decades in summer and both distributions are approximately lognormal over much of their range. Probability plots using $\log_{10}(L)$ for the abscissa are shown in Fig. 6d; the plot should be linear if the variable is lognormal. In winter the $\log_{10}(L)$ distribution is linear between 2%

and 90% cumulative probability while in summer the distribution is linear between 5% and 75% cumulative probability.

5. Inferring vertical mixing rates for Juan de Fuca Strait

The Thorpe scale L_T is essentially the rms vertical length scale of density inversions. On dimensional, or energetic grounds, it is expected to be proportional to the Ozmidov scale, $L_o = (\epsilon/N^3)^{1/2}$, where ϵ is the dissipation rate of kinetic energy. Dillon (1982) and Crawford (1986) find that $L_o \approx 0.8 L_T$, so, with $K_v = 0.2 L_o^2 N$ (Oakey 1982), we expect that the eddy diffusivity $K_v \approx 0.1 L_T^2 N$, the form of which is dimensionally inevitable.

Seventeen coincident microstructure velocity shear and temperature profiles were collected in Juan de Fuca Strait in August 1996 (see Fig. 7) and provided independent estimates of L_o and L_T . The microstructure profiler was equipped with two shear probes, a fast and slow temperature probe, a conductivity sensor, and a

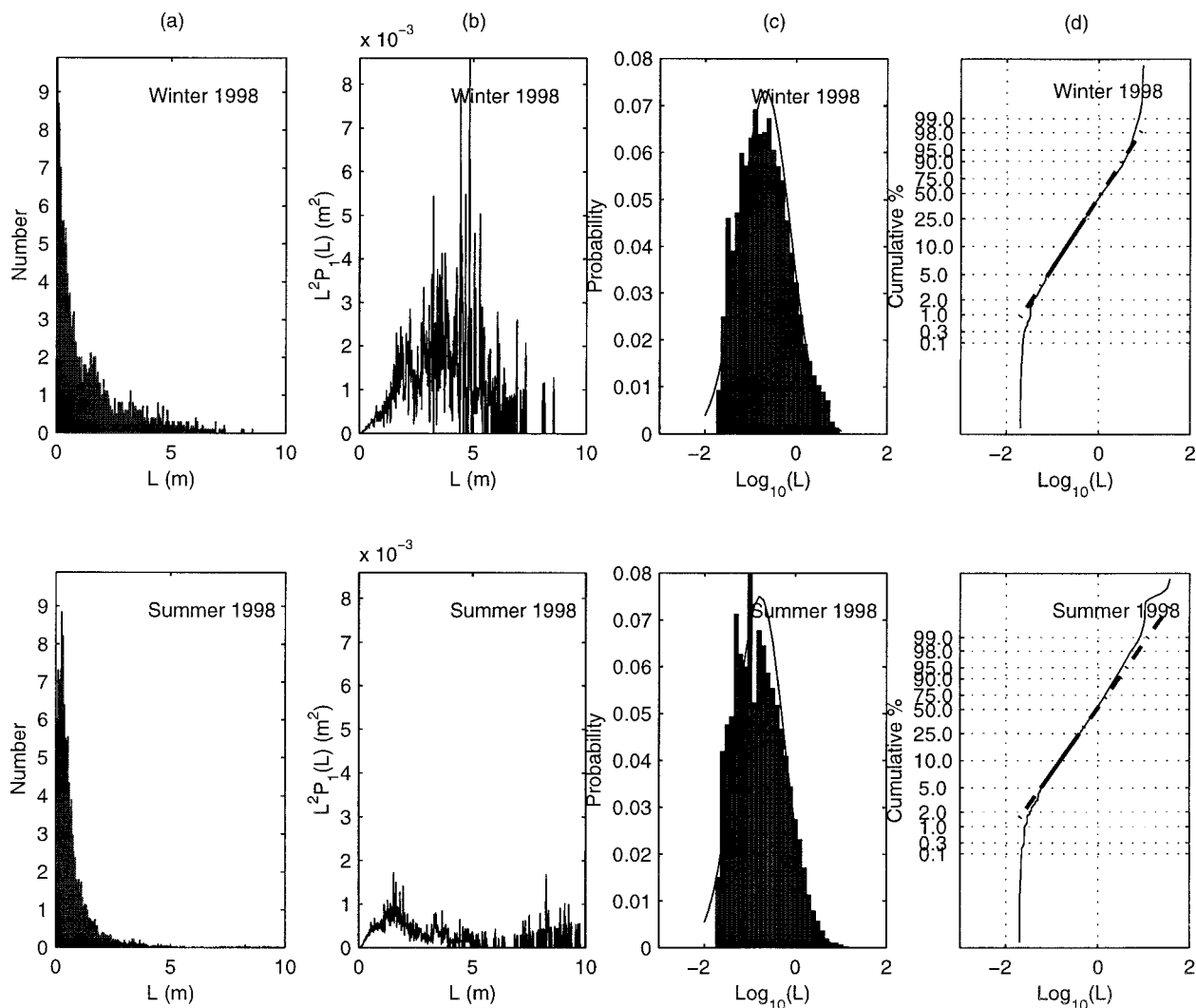


FIG. 6. (a) Mean histogram of L (the occurrence of $L = 0$ has not been plotted), (b) mean distribution of $L^2 P_1(L)$, (c) histogram of $\log_{10}(L)$, and (d) cumulative probability plot of $\log_{10}(L)$, calculated from midwater potential density profiles from the CT1 sensor pairs. The winter distributions are the average of 10 casts and the summer distributions are the average of 57 casts. The corresponding rms midwater Thorpe scales $\overline{L_{T_{wc}}^2}^{1/2}$ are 0.77 m for the winter data and 0.45 m for the summer data.

pressure gauge (Dewey et al. 1987). The fast sensors (shear-1, shear-2, and fast temperature) had a sampling rate of 248 s^{-1} while the slow sensors (T, C, and P) had a sampling rate of 31 s^{-1} . Unfortunately the fast temperature sensor and the conductivity sensor did not work properly and will not be discussed further. The shear probes were calibrated in the Ocean Turbulence Laboratory at the University of Victoria prior to the deployment.

The microstructure shear was calculated from

$$\frac{du}{dz} = \frac{S_c V_c}{GW^2},$$

where S_c is the shear probe calibration, V_c is the voltage signal, G is the shear channel gain, and W is the fall speed. The dissipation rate, ϵ (J kg^{-1}) was then calculated from the despiked shear data using the relationship,

$$\epsilon \equiv \frac{15}{2} \nu \overline{\left(\frac{\partial u}{\partial z}\right)^2},$$

where ν is the molecular viscosity of seawater at the local temperature. The variance of the shear data was calculated, following Dewey et al. (1987), by integrating the power spectrum between 1 and 50 s^{-1} to remove noise in the shear data.

Estimates of $L_{T_{ovt}}$ were made from the slow temperature profiles using only the part of the water column where the T - S relationship was monotonic. This T - S region was found from two CTD casts: one taken immediately before and one immediately after the microstructure profiling, which lasted for three hours.

Values of $L_{O_{ovt}}$ were calculated as by Dillon (1982) and Crawford (1986), using the relationship $L_{O_{ovt}} = (\overline{\epsilon}/N^3)^{1/2}$,

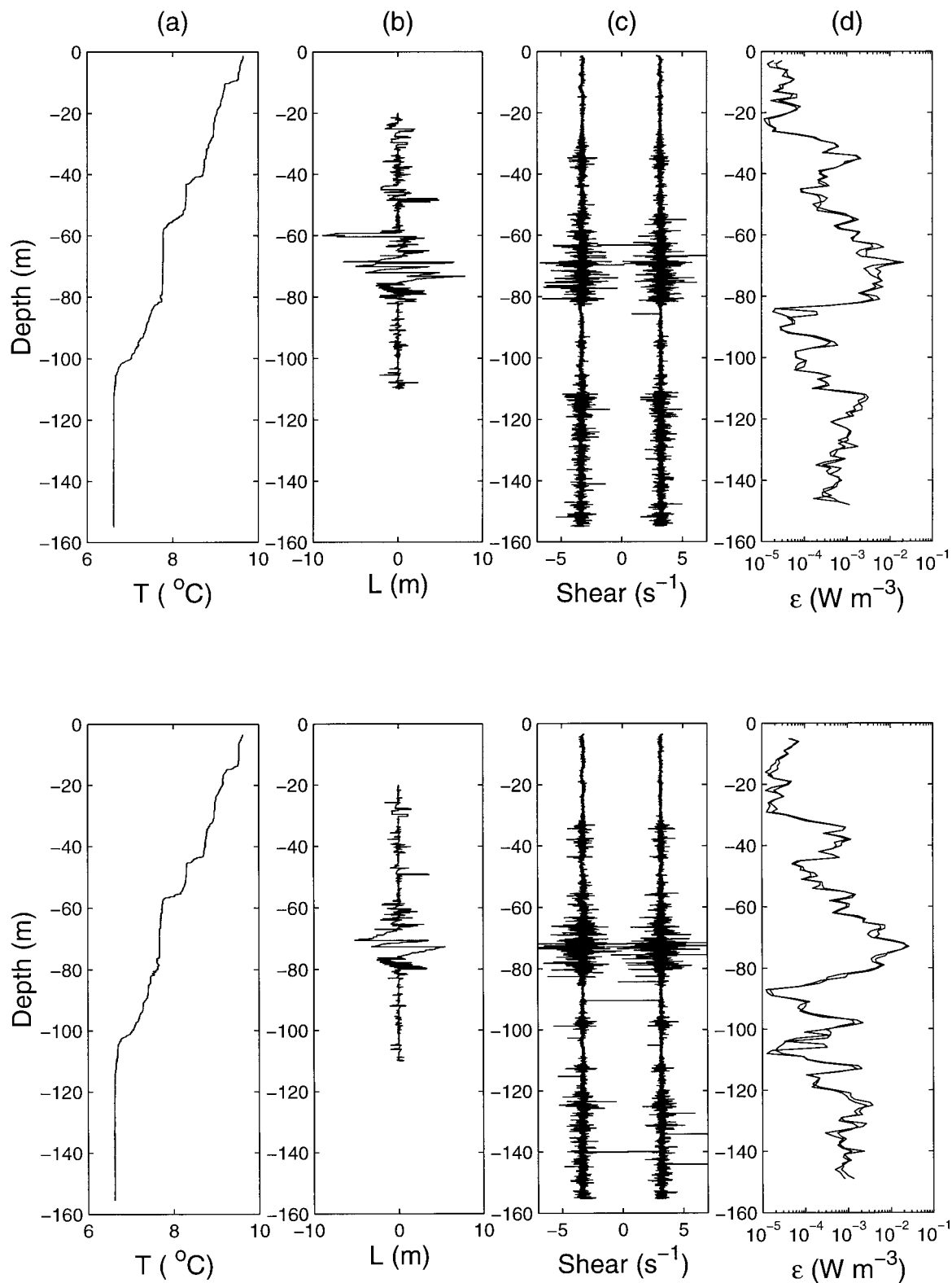


FIG. 7. Examples of temperature and velocity shear data from two airfoil shear probes collected in Juan de Fuca Strait during Aug 1996: (a) cleaned temperature, (b) Thorpe displacement from the part of the water column where the T - S relationship is monotonic, (c) shear, and (d) dissipation rate.

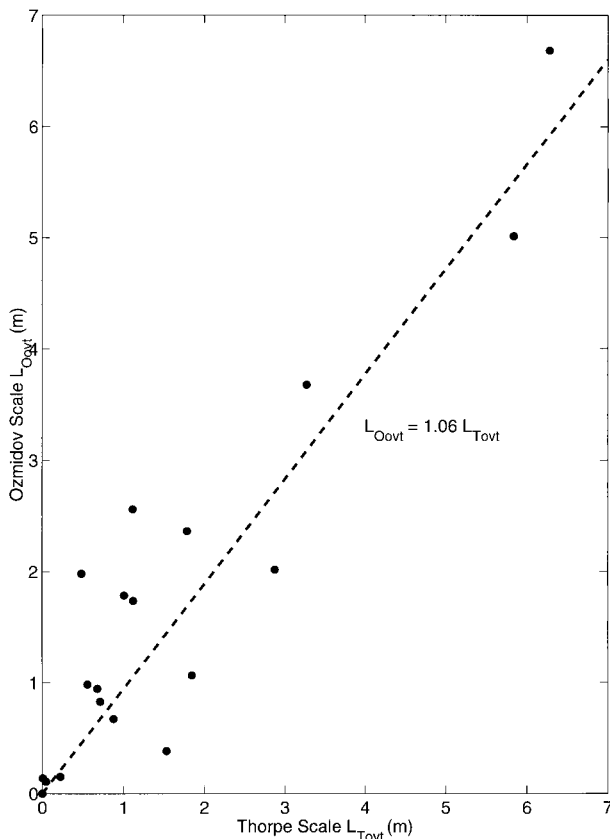


FIG. 8. The relationship between L_{Oovt} and L_{Tovt} calculated from microstructure shear and temperature data collected in Juan de Fuca Strait in Aug 1996. The regression shown minimizes the function $\sum_{i=1}^n |y_i - bx_i|$ (Press et al. 1989). Data from 19 overturns were used to compute L_{Oovt} and L_{Tovt} .

where $\bar{\epsilon}$ is the mean dissipation rate and \bar{N} is the mean value of the buoyancy frequency over each overturn from the reordered stable potential density profile. Using the values of L_{Oovt} and L_{Tovt} calculated from the microstructure data we found $L_{Oovt} \approx 1.06 L_{Tovt}$, in close agreement with the relationship found by Dillon (1982) and Crawford (1986); see Fig. 8.

Ott and Garrett (1998) estimated an eddy viscosity $A_v \approx 0.02 \text{ m}^2 \text{ s}^{-1}$ for Juan de Fuca Strait based on a balance between the along-strait pressure gradient and internal friction. If one believes that this sets a lower bound for the dissipation rate (as it includes the contribution from the mean shear alone), $\epsilon \geq (1 - R_f)A_v(d\bar{u}/dz)^2$, where $R_f \approx 0.15$ is the flux Richardson number. For a mean vertical shear of 0.007 m s^{-1} and summer stratification $N \approx 0.012 \text{ s}^{-1}$, L_{Twc} should exceed 0.7 m. Our CTD observations show that, on average, the measured L_{Twc} in August 1998 is considerably less than this value. Conversely, the mean “midwater” column dissipation rate $\langle \epsilon \rangle$ calculated from $\langle \epsilon \rangle = 0.64 \bar{N}^3 L_{Twc}^2$ suggests that $A_v \leq 0.005 \text{ m}^2 \text{ s}^{-1}$. The discrepancy between our measurements and the estimate of Ott and Garrett (1998) could be associated with time var-

iability, but our data were obtained near mean slack neap tide, precisely the condition which Ott (2000) and Ott et al. (2001, manuscript submitted to *J. Phys. Oceanogr.*) found was associated with the largest values of the Reynolds stresses within the stratified region of the shear flow.

We also find that on average 12% of the water column was overturning in February but only 2% was overturning in August. The reason for this is not clear as we have no evidence for dramatic seasonal differences in the mean bulk Richardson number (S. Mihaly 2000, personal communication), though of course on any given day the situation could be far from the seasonal mean.

Because of the sparseness of our data in space and time, and the strong tidal currents in Juan de Fuca Strait, it is not reasonable to discuss the profile to profile variations in the mixing rate calculated from the data. However, using the empirical relationship between L_{Tovt} and L_{Oovt} , extending it to the whole water column and using our mean values of $\bar{N}L_{Twc}^2$, we estimate that the average value of K_v is $5 \times 10^{-4} \text{ m}^2 \text{ s}^{-1}$ in February and $2 \times 10^{-4} \text{ m}^2 \text{ s}^{-1}$ in August 1998.

6. The distribution of $P_3(L/H)$

As shown by (2), $P_1(L)$ is a convolution of the probability distribution of overturn height, $P_2(H)$, with the probability distribution of the fractional displacement within each overturn, $P_3(L/H)$. The distributions of $P_2(H)$, Fig. 9, show a preponderance of small values of H . Similarly, Gregg et al. (1986) and Yamazaki and Lueck (1987) found that thin turbulence patches were more common than thick patches, based on an analyses of temperature microstructure data. They also noted that thick patches had much higher dissipation rates than thin patches and therefore were significant contributors to the total mixing rate. From probability plots (not shown) we found that the $\log_{10}(H)$ distribution is almost linear (implying lognormality) between the 5% and 50% levels in winter and between the 2% and 75% levels in summer, although we have only a small number of measurements of H in each case.

We have no theoretical prediction with which to compare the distribution of $P_2(H)$, neither do we have sufficient data to check the assumption that $P_3(L/H)$ is independent of H . Proceeding with this assumption, however, Fig. 10 shows $P_3(L/H)$ for all observed overturns in winter and summer. As a first step in exploring the shape of this distribution, we compare it with a simple kinematic model in which every point in a profile has an equal probability of having a displacement to every other point. This is the same as assuming that each possible rearrangement of the original profile is equally likely.

We illustrate this with a set of five points, representing points on a stable density profile (i.e., 1, 2, 3, 4, 5) and consider that the points have been reordered from some previous density profile (such as 5, 3, 4, 1, 2). If each

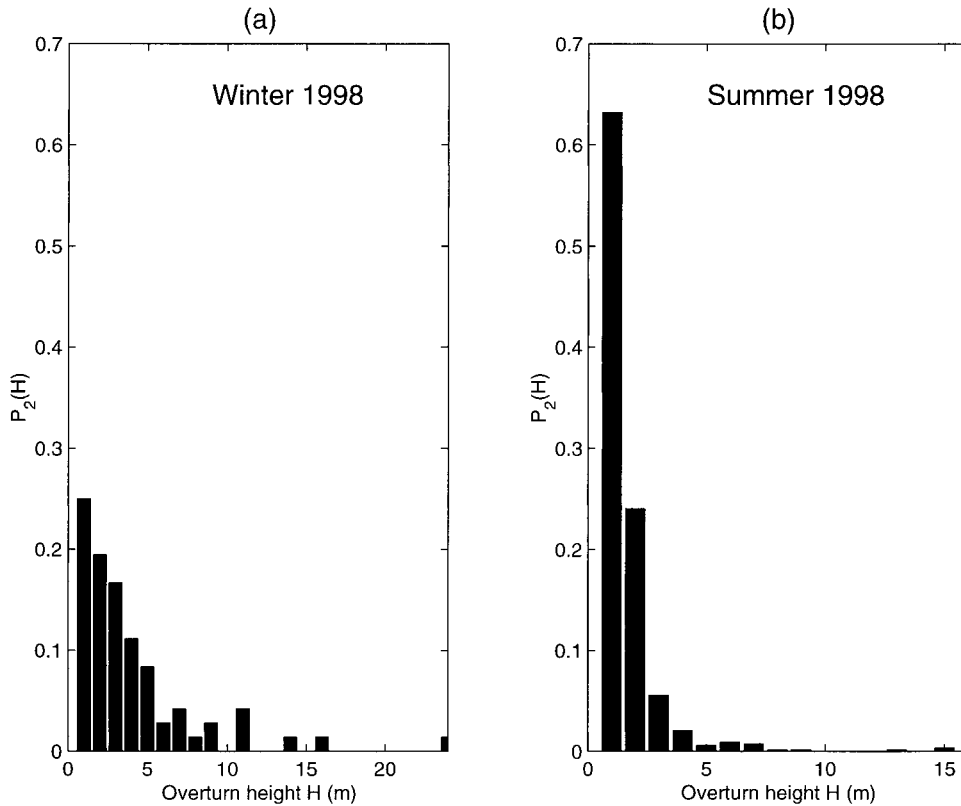


FIG. 9. Mean distribution of $P_2(H)$ for (a) winter and (b) summer.

point can previously have been at any other point, then we can construct a matrix showing how many chances each point has of being moved from m places away, where $m = 0$ to 4. For a set of five points, the matrix is given below:

Point number n	Move of m places				
	0	1	2	3	4
1	1	1	1	1	1
2	1	2	1	1	0
3	1	2	2	0	0
4	1	2	1	1	0
5	1	1	1	1	1
Total	5	8	6	4	2

Then, the probability of each displacement $m = 0, 1, 2, 3, 4$, is $5/25, 8/25, 6/25, 4/25$, and $2/25$ respectively. Thus, for an arbitrary set of n points the probability of zero displacement ($m = 0$) is n/n^2 , and the probability of a displacement of one unit or more ($m = 1, \dots, 4$) is $2(n - m)/n^2$. Using (1), the square of the Thorpe scale is then just

$$L_T^2 = \frac{1}{6} H^2 \left(1 - \frac{1}{n^2} \right), \tag{4}$$

where H is the overturn height. For large n , $L_T^2 = \frac{1}{6} H^2$.

Figure 10 shows the model distribution for a set of

50 points, normalized to lie between 0 and 1, superimposed on our mean distributions of $P_3(L/H)$. The data have a larger probability of small L/H , but a smaller probability of medium to large L/H than the simple model.

For each set of n points, however, there is a subset of combinations that do not represent an n -point overturn, but instead represent an overturn, or multiple overturns, which have length less than n . This set includes, but is not limited to, those cases where $1 \rightarrow 1$ and $n \rightarrow n$, for example. For $n = 5$, there are 49 such combinations, out of a total of 120, which do not represent a 5 point overturn, leaving 71 that do. In general, while there are $n!$ rearrangements of n points, the number $F(n)$ which represent a complete n -point overturn is given by the recurrence relation¹

$$F(n) = n! - \sum_{k=1}^{n-1} k! F(n - k) \quad \text{for } n \geq 2. \tag{5}$$

We have subtracted from $n!$ the number $k!$ of rearrangements of the first k points times the number of complete overturns in the remaining $n - k$ points, and then sum this from $k = 1$ to $n - 1$. While a 1 point

¹ We confess that the derivation of (5) did not occur to us immediately, but a Monte Carlo computer simulation led us to the integer sequence (Sloane and Plouffe 1995, integer sequence M2948) and hence to a reference for the recurrence relation (Comtet 1972).

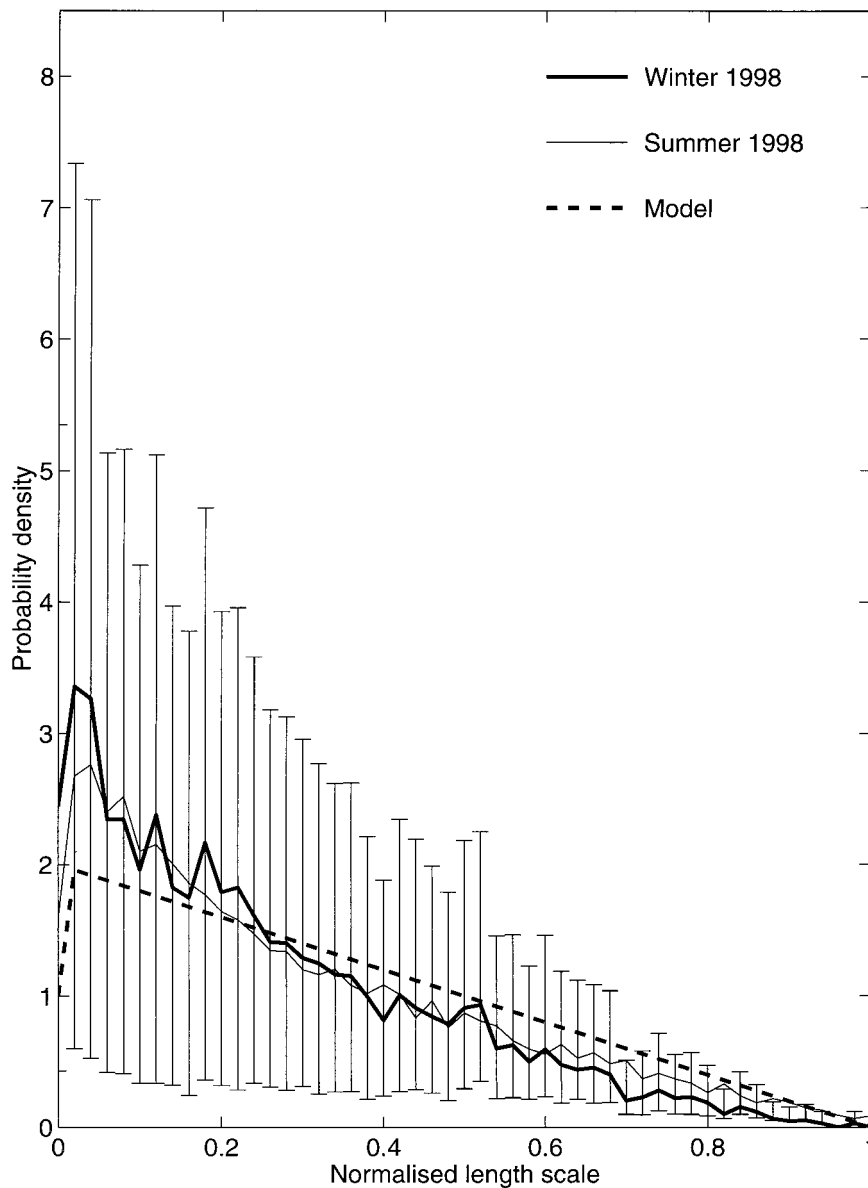


FIG. 10. Mean distribution of $P_3(L/H)$ for all observed overturns in winter and summer and the normalized distribution from the model for a set of 50 points. The error bars shown are the 95% confidence intervals for the winter data based on a bootstrap method using 1000 iterations; error bars for the summer data are similar in magnitude.

overturn is undefined, we must choose $F(1) = 1$ to have (5) give $F(2) = 1$ correctly.

It can be seen from Fig. 11 that, when n is small, the restriction of considering only n -point overturns reduces the probability of moving a small number of places, but increases the chance of moving a large number of places. As n tends to infinity, the distribution approaches that of the original unrestricted model. In our dataset, there are typically tens of points in each overturn (this depends on the instrument resolution of course), so the unrestricted model is an appropriate benchmark.

In the unrestricted case discussed first, with $n!$ rear-

rangements of n points, the number of displacements by m points is $M(n, m)$, where

$$\begin{aligned} M(n, 0) &= n! \quad \text{and} \\ M(n, m) &= 2(n - m)(n - 1)! \\ &\quad \text{for } m = 1, \dots, n - 1. \end{aligned} \quad (6)$$

The total number of displacements is $n \times n!$. Dividing $M(n, m)$ by this gives the probabilities previously cited.

For the restricted case, excluding those that do not represent a complete overturn, the number of displace-

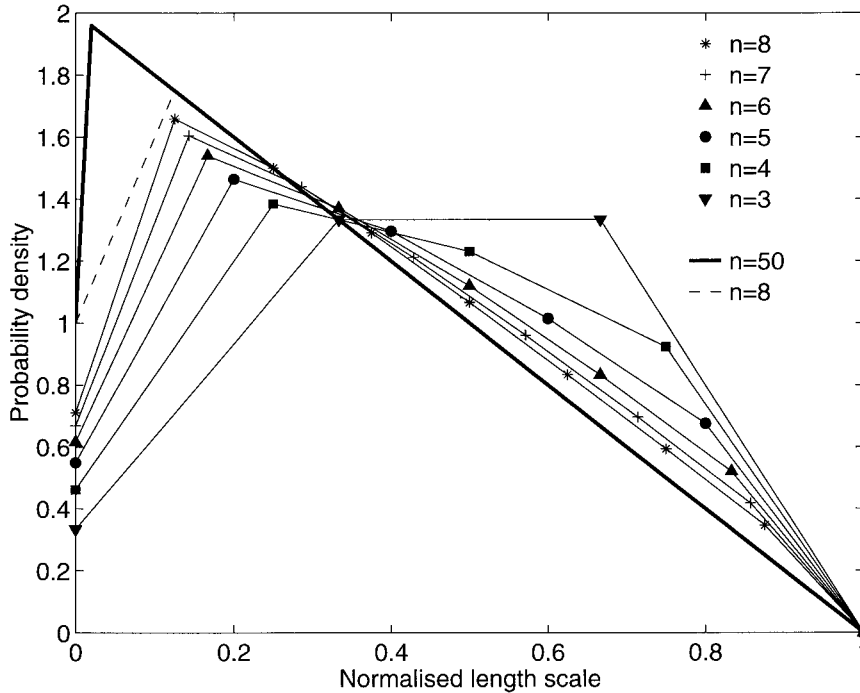


FIG. 11. Normalized probability distributions of the modified kinematic model for $n = 3, 4, 5, 6, 7,$ and 8 (lines with symbols) taking into account only n -point overturns, and the original kinematic model distribution for a set of 8 and 50 points (lines without symbols), also normalized.

ments by m points is now given by the recurrence relation

$$N(n, m) = M(n, m) - \sum_{k=1}^{n-m-1} k!N(n - k, m) - \sum_{k=m+1}^{n-1} F(n - k)M(k, m). \tag{7}$$

The first correction to $M(n, m)$ removes, for each k , $k!$ times the number of complete overturns in the remaining $n - k$ points, as in the derivation of (5). We must also remove all the unrestricted possibilities in the first k points, multiplied by the number $F(n - k)$ of complete overturns in the remaining $n - k$ points. As for $F(1)$, we must take $N(1, 0) = 1$ to initiate (7). We have checked the result of (7) by computer evaluation, though this becomes lengthy for $n \geq 8$.

The probability $P(n, m)$ of displacement by m points in an n point overturn is just

$$P(n, m) = N(n, m)/nF(n). \tag{8}$$

For $n = 5$, it leads to $P(n, m) = 0.11, 0.29, 0.26, 0.20,$ and 0.14 instead of $0.20, 0.32, 0.24, 0.16,$ and 0.08 for $m = 0, 1, 2, 3, 4$.

The shape of the probability distributions from our data is rather uncertain as shown by error bars in Fig. 10, which represent the 95% confidence interval about the mean, calculated using a bootstrap method with 1000 iterations. The smoothness of the final curves in Fig.

10, however, suggests much smaller error bars. The simple kinematic model distribution (Figs. 10, 11) somewhat resembles the mean distribution from the data, though the data do show a preference for more small displacements than given by our simple model. This could be the effect of molecular diffusion; it would be interesting to compare our findings with $P_3(L/H)$ from direct numerical simulation of, say, Kelvin–Helmholtz instability.

The shape of the probability distribution function of the normalized Thorpe displacement might depend on the situation (circumstance or location?) but it is not known what the external nondimensional parameters are. By averaging data from many overturns we hope that we have included measurements from all stages of instability, so the shape of the probability distribution function averages out any time dependence. The shape may also depend on the instability mechanism; here we assume shear instability is the main process. Possible relevant nondimensional parameters could be (i) the minimum Richardson Number achieved and (ii) the length of time for which the Richardson number is less than 0.25 compared with the Brunt–Väisälä period. We suggest that the shapes of $P_3(L/H)$ and $P_2(H)$ are worthy of further investigation both observationally and theoretically.

7. Conclusions

We conclude that the Thorpe scale in Juan de Fuca Strait was about 0.77 m in February and 0.45 m in

August 1998 and that frequent small overturns do not contribute significantly to the estimate of the mean Thorpe scale. We have reliably detected values of K_v , as small as $2 \times 10^{-4} \text{ m}^2 \text{ s}^{-1}$ with an “off the shelf” CTD. We believe that better results could be obtained with a CTD that is decoupled from ship motion (i.e., free fall) and with a finer resolution pressure sensor (i.e., one with a full scale pressure range suited to coastal water depths as opposed to midocean water depths). The CTD measurements are biased toward large Thorpe displacements so that detailed interpretations of the calculated mixing rates must consider whether sufficient samples to give adequate statistics have been obtained.

We have introduced various probability distributions. One, the distribution $P_2(H)$ of overturn height, falls off rapidly with increasing H though we lack a theory for its shape. The probability distribution $P_3(L/H)$ of scaled displacements within overturns shows rather more small displacements than given by a kinematic model in which all possible contributions are equally likely. The probability $P_1(L)$ of displacements is a convolution of $P_2(H)$ and $P_3(L/H)$. More investigation of these concepts would seem to be worthwhile.

Acknowledgments. The authors thank Dr. Tom Sanford who provided the opportunity to collect the February data as part of the one-day shipboard training course for the graduate class in “Methods and Measurements in Physical Oceanography” at the University of Washington. We also thank the Institute of Ocean Sciences, Sidney, B.C., for the loan of the SBE 911plus CTD for the August cruise, and Dr. Rolf Lueck for providing calibration facilities for the microstructure shear probes. We are very grateful to two anonymous reviewers for critical and helpful comments. This project was supported by the U.S. Office of Naval Research and the Natural Sciences and Engineering Research Council, Canada.

REFERENCES

- Alford, M., and R. Pinkel, 2000: Observations of overturning in the thermocline: The context of ocean mixing. *J. Phys. Oceanogr.*, **30**, 805–832.
- Comtet, L., 1972: Sur les coefficients de l'inverse de la série formelle $\sum n!t^n$. *C. R. Acad. Sci. Paris, Série A*, **275**, 569–572.
- Crawford, W. R., 1986: A comparison of length scales and decay times of turbulence in stably stratified flows. *J. Phys. Oceanogr.*, **16**, 1847–1854.
- Dewey, R. K., W. R. Crawford, A. E. Gargett, and N. S. Oakey, 1987: A microstructure instrument for profiling oceanic turbulence in coastal bottom boundary layers. *J. Atmos. Oceanic Technol.*, **4**, 288–297.
- Dillon, T. M., 1982: Vertical overturns: A comparison of Thorpe and Ozmidov scales. *J. Geophys. Res.*, **87**, 9601–9613.
- Ferron, B., H. Mercier, K. Speer, A. Gargett, and K. Polzin, 1998: Mixing in the Romanche Fracture Zone. *J. Phys. Oceanogr.*, **28**, 1929–1945.
- Fofonoff, P., and R. C. Millard, 1983: Algorithms for computation of fundamental properties of seawater. UNESCO Tech. Paper in Mar. Sci., No. 44, 53 pp.
- Frisch, U., 1995: *Turbulence*. Cambridge University Press, 310 pp.
- Galbraith, P. S., and D. E. Kelley, 1996: Identifying overturns in CTD profiles. *J. Atmos. Oceanic Technol.*, **13**, 688–702.
- Gregg, M. C., E. A. D'Asaro, T. J. Shay, and N. Larson, 1986: Observations of persistent mixing and near-inertial internal waves. *J. Phys. Oceanogr.*, **16**, 856–885.
- Lueck, R. G., and J. J. Picklo, 1990: Thermal inertia of conductivity cells: Observations with a Sea-Bird cell. *J. Atmos. Oceanic Technol.*, **7**, 756–768.
- Morison, J., R. Anderson, N. Larson, E. D'Asaro, and T. Boyd, 1994: The correction for thermal-lag effects in Sea-Bird CTD data. *J. Atmos. Oceanic Technol.*, **11**, 1151–1164.
- Mudge, T. D., and R. G. Lueck, 1994: Digital signal processing to enhance oceanographic observations. *J. Atmos. Oceanic Technol.*, **11**, 825–836.
- Oakey, N. S., 1982: Determination of the rate of dissipation of turbulent energy from simultaneous temperature and velocity shear microstructure measurements. *J. Phys. Oceanogr.*, **12**, 256–271.
- Ott, M. W., 2000: Mixing and secondary circulation in Juan de Fuca Strait. Ph.D. thesis, University of Victoria, 162 pp.
- , and C. Garrett, 1998: Frictional estuarine flow in Juan de Fuca Strait, with implications for secondary circulation. *J. Geophys. Res.*, **103**, 15 657–15 666.
- Ozmidov, R. V., 1965: On the turbulent exchange in a stably stratified ocean. *Izv. Acad. Sci. USSR, Atmos. Oceanic Phys.*, **1**, 861–871.
- Press, W. H., B. P. Flannery, S. A. Teukolsky, and W. T. Vetterling, 1989: *Numerical Recipes, The Art of Scientific Computing*. Cambridge University Press, 702 pp.
- Sea-Bird Electronics, Inc., 1992: Fundamentals of the TC Duct and pump-controlled flow used in Sea-Bird CTDs. Sea-Bird Application Note 38, 5 pp.
- Sloane, N. J. A., and S. Plouffe, 1995: *The Encyclopedia of Integer Sequences*. Academic Press, 587 pp.
- Thorpe, S. A., 1977: Turbulence and mixing in a Scottish Loch. *Philos. Trans. Roy. Soc. London*, **286A**, 125–181.
- Yamazaki, H., and R. Lueck, 1987: Turbulence in the California undercurrent. *J. Phys. Oceanogr.*, **17**, 1378–1396.